**Earth Surface Processes and Landforms**
*Earth Surf. Process. Landforms* **33**, 380–393 (2008)
Published online in 8 August 2007 Wiley InterScience
(www.interscience.wiley.com) **DOI:** 10.1002/esp.1562

# GIS-based regional landslide susceptibility mapping: a case study in southern California

Yiping He and R. Edward Beighley*
*San Diego State University, Civil and Environmental Engineering, San Diego, CA, USA*

**Correspondence to: Civil and Environmental Engineering, San Diego State University, 5500 Campanile Drive, San Diego, CA 92182, USA.*
*E-mail: beighley@mail.sdsu.edu*

Received 19 September 2006;
Revised 9 May 2007;
Accepted 23 May 2007

## Abstract

**Landslides threaten lives and property throughout the United States, causing in excess of $2 billion in damages and 25–50 deaths annually. In regions subjected to urban expansion caused by population growth and/or increased storm intensities caused by changing climate patterns, the economic and society costs of landslides will continue to rise. Using a geographic information system (GIS), this paper develops and implements a multivariate statistical approach for mapping landslide susceptibility. The presented susceptibility maps are intended to help in the design of hazard mitigation and land development policies at regional scales. The paper presents (a) a GIS-based multivariate statistical approach for mapping landslide susceptibility, (b) several dimensionless landslide susceptibility indexes developed to quantify and weight the influence of individual categories for given potential risk factors on landslides and (c) a case study in southern California, which uses 11 111 seismic landslide scars collected from previous efforts and 5389 landslide scars newly digitized from local geologic maps. In the case study, seven potential risk factors were selected to map landslide susceptibility. Ground slope and event precipitation were the most important factors, followed by land cover, surface curvature, proximity to fault, elevation and proximity to coastline. The developed landslide susceptibility maps show that areas classified as having high or very high susceptibilities contained 71% of the digitized landslide scars and 90% of the seismic landslide scars while only occupying 26% of the total study area. These areas mostly have ground slopes higher than 46% and 2-year, 6-hour precipitation greater than 51 mm. Only 12% of digitized landslides and less than 1% of recorded seismic landslides were located in areas classified as low or very low susceptibility, while occupying 42% of the total study region. These areas mostly have slopes less than 27% and 2-year, 6-hour precipitation less than 41 mm. Copyright © 2007 John Wiley & Sons, Ltd.**

**Keywords: landslide; susceptibility; risk; map; southern California; GIS**

## Introduction

Landslides are among the most widespread geological hazards on earth and threaten lives and property globally. In the United States, it is estimated that landslides cause more than $2 billion in damages and 25–50 deaths annually (National Research Council, 2004). Despite advances in science and technology, these events continue to result in human suffering, property loss and environmental degradation. As regional populations, urban expansion and storm intensities increase due to changing development and climate patterns, the economic and society costs of landslides will continue to rise, increasing the demand for improved protection against landslides. Landslide susceptibility mapping is a valuable tool for assessing current and potential risks that can be used for developing early warning systems, mitigation plans and land use restrictions.

In the last three decades, landslide susceptibility mapping has become a topic of major interest for both geoscientists and engineering professionals as well as the community and local officials in many parts of the world. Various techniques or tools have been adopted for determining landslide susceptibility. General overviews can be found in the work of Leroi (1997), Aleotti and Chowdhury (1999), Guzzetti *et al.* (1999), Dai *et al.* (2002) and Van Westen (2004). All of these approaches can be divided into two groups: qualitative and/or semi-quantitative methods and

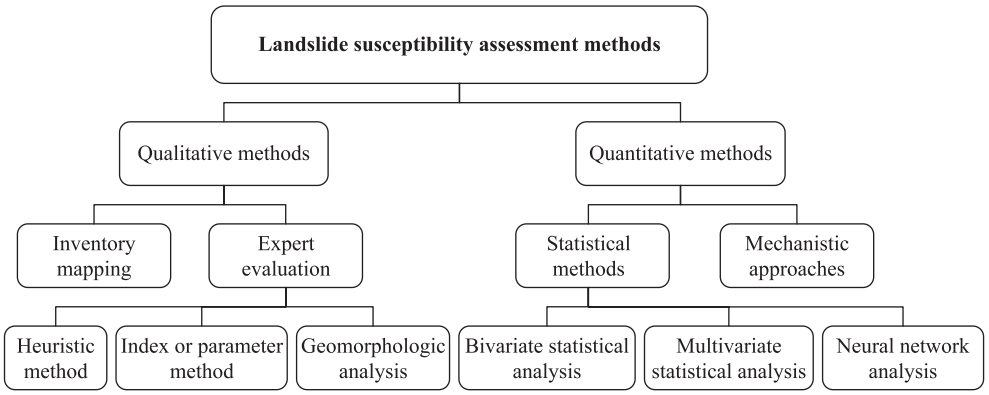


**Figure 1.** Proposed classification of landslide susceptibility assessment methods.

quantitative methods (Figure 1). The qualitative and/or semi-quantitative methods can include inventory mapping and expert evaluations. The quantitative methods can include statistical and mechanistic methods.

Landslide inventory maps are commonly prepared by collecting historic information on landslide events from aerial photograph and satellite images. The inventories are an elementary form of susceptibility mapping because they emphasize the location and extent of recorded landslides. However, landslide inventory maps do not identify areas that may be susceptible to landslides unless landslides have already occurred. The challenge in susceptibility mapping is developing a powerful system from limited inventories (Dai *et al.*, 2002).

Expert evaluation can include heuristic methods, geomorphologic analysis and index or parameter methods. In heuristic methods, expert opinions are used to estimate landslide potential from data on potential risk factors (or variables), based on the assumption that the relationships between landslide susceptibility and the risk factors are known and can be specified by models (Gupta and Joshi, 1989; Dai *et al.*, 2002). Geomorphologic analysis is probably the simplest of the qualitative methods and was used frequently in the 1970s and 1980s (Fenti *et al.*, 1979; Kienholz, 1978; Rupke *et al.*, 1988). The assessment is rapidly carried out in the field by qualified scientists based on their experience in similar situations. In the index or parameter approach, the expert selects and maps the factors that affect slope stability and assigns a weighted value to each factor that is proportionate to its expected relative contribution in generating failure, based on personal experience (Anbalagan and Singh, 1996; Gupta and Anbalagan, 1997; Wachal and Hudak, 2000; Morton *et al.*, 2003). Expert evaluation is the most widely used approach for landslide hazard evaluation and can be used successfully at any scale. Its main disadvantages are subjectivity in the process of decision making, long-term information required on landslides and lengthy field surveys (Carrara, 1983; Van Westen *et al.*, 1997).

Statistical methods were developed to overcome the relatively high level of subjectivity related to expert evaluation (Fall *et al.*, 2006). They involve the statistical assessment of combinations of factors that have caused landslides in the past. Quantitative or semi-quantitative estimates are then performed for areas not affected by landslides, but where the same conditions exist (Dai *et al.*, 2002). Statistical methods are generally considered the most appropriate method for landslide susceptibility mapping at regional scales because they are objective, reproducible and easily updatable (Naranjo *et al.*, 1994). Several groups (Carrara, 1983; Bernknopf *et al.*, 1988; Aleotti *et al.*, 1998; Atkinson and Massari, 1998; Guzzetti *et al.*, 2005) have applied bivariate or multivariate statistical methods to evaluate the landslide hazards successfully. Two drawbacks with the use of statistical methods are that (1) indicator factors are selected by expert or personal opinion and (2) data are required over large spatial and temporal extents. It is often problematic to carry out detailed data gathering at acceptable costs (Van Westen *et al.*, 1997).

Building on traditional statistical methods, artificial neural networks (ANNs) provide statistically based, computational tools for organizing and correlating information in ways that have proved useful for solving complex, poorly understood and/or resource-intensive problems (Chang and Liu, 2004). Several efforts (Aleotti *et al.*, 1998; Lee *et al.*, 2003) have applied ANN analysis to evaluate landslide susceptibility successfully. ANNs have advantages compared to traditional statistical methods: (a) ANN methods are independent of the statistical distribution of the data; (b) there is no need for a specific statistical factor (or variable) and (c) accurate analysis is possible with only a few training datasets. ANN disadvantages are (a) that resultant values do not accurately coincide with the correct values because initial weights are random, (b) that factors are selected empirically and (c) lengthy execution time (Lee *et al.*, 2003).

Mechanistic approaches evaluate and analyze slope stability using deterministic or probabilistic models. These models (one, two or three dimensional) are commonly used for small areas at fine scales and/or in soil engineering for slope-specific stability studies (Ward *et al.*, 1981; Wilson and Keefer, 1983; Nash, 1987; Terlien *et al.*, 1995; Jibson



DOI: 10.1002/esp

*et al.*, 1998; Jibson, 2001; Collins and Znidarcic, 2004). In this type of approach, soil properties are used to calculate a factor of safety based on an infinite slope stability analysis, such as SINMAP (Pack *et al.*, 1999), SHALSTAB (Montgomery and Dietrich, 1994), LISA (Hammond *et al.*, 1992) and the transient response model (Iverson, 2000). The advantage of these methods is their physically based framework. Due to the high spatial variability of geotechnical parameters and the laborious methods involved in acquiring these data, the approximation of model parameters is practically limited to site investigations (Van Westen *et al.*, 1997). In landslide susceptibility or hazard assessment over large areas, mechanistic methods are commonly limited to only studying the stability of slopes (Fall *et al.*, 2006).

The review of different methods for landslide susceptibility mapping discussed above has shown that all available techniques present both advantages and disadvantages. The successful use of one method or another strongly depends on many factors, such as the mapping scale, accuracy of expected results and data availability. For a regional scale landslide susceptibility assessment, statistical methods may be the most applicable because they are relatively simple to implement, provide quantitative results and are easily updated. However, traditional statistical methods still lack the ability to quantify the influence of individual factors and their different categories. In recent years, geographical information systems (GISs) have proven to be a versatile tool for the display, analysis, management and modeling of spatial data. Through appropriate use of GISs, most approaches to landslide susceptibility mapping enable total automation of assessment and the standardization of data management techniques, from acquisition through final analysis (Soeters and Van Westen, 1996; Stevenson, 1977; Anbalagan and Singh, 1996).

This paper presents a GIS-based multivariate statistical approach for regional landslide susceptibility assessment. The approach is applied to map landslide susceptibility in southern California using a newly digitized landslide inventory (extent and location). The main objectives of this paper are to (1) generate dimensionless indexes to quantify the susceptibility of landslides within selected indicator categories, (2) develop indexes to weight the influence of selected indicator parameters on the occurrence of landslides, (3) present a GIS-based mapping approach for landslide susceptibility in southern California and (4) develop GIS data that describes the extent and location of landslides in selected regions of southern California.

## Study Region

The region includes 33 220 km$^2$ or roughly 8% of the land area in California, and is comprised of three sub-regions (not including the Channel Islands): South Coast, Transverse Ranges and Peninsular Ranges (Figure 2). The region is bounded by the transition to the Mojave Desert to the east, the Pacific Ocean to the west, the Tehachapi Mountains to the north and the US–Mexico border to the south. The region is located along or near the boundary between the largest tectonic plate on the earth's crust (the Pacific Plate) and the continental North American Plate. There are a variety of active faults, and earthquakes and landslides are common. The mean elevation is 615 m (2020 ft) above sea level, ranging from sea level to 3480 m (11 420 ft). Approximately half the region has ground slopes greater than 50% (27°), and a third has slopes greater than 70% (35°). Because of the contrast between the ocean and continental air masses and the great differences in elevation and slope, the region displays a large diversity in weather and climate. The mean annual precipitation is 432 mm (17 in), ranging from 229 mm (9 in) to 1295 mm (51 in).

Based on 1990s land use/land cover data, the region is comprised of approximately 28% urban lands, 66% undeveloped areas and 6% agricultural lands. In recent decades, southern California has experienced extraordinarily rapid population growth. Based on 1980 and 2000 census data, 18·7 million people (55% of California's total population) reside in this region. From 1980 to 2000, the population increased at a rate of 41%, of which, Riverside, San Diego, Orange, Ventura, Santa Barbara and Los Angeles Counties grew by 133, 51, 47, 42, 34 and 27%, respectively. It is this rapid urbanization, particularly in the low-lying coastal regions, that is causing increasing activities and loss by mass movements in the region. Landslides or other mass wasting processes occur widely on steep slopes triggered by intense rainfall, likely due to the powerful tectonic movements, earthquake activity, deforestation by urbanization and weathering producing an abundance of loose regolith and soil. As a result, the region provides an ideal setting for studying landslides (Selby, 2000).

## Methodology

Landslide susceptibility is the probability that a region will be affected by landslides, given a set of environmental conditions (Brabb, 1984). In this paper, susceptibility, *S*, was used to quantify the probabilities of individual categories (or subclasses) for potential risk factors contributing to landslide occurrence in a given region. For example, factors such as land cover, elevation, civil infrastructure, ground slope, aspect, tectonic and lithology are commonly recognized as



DOI: 10.1002/esp

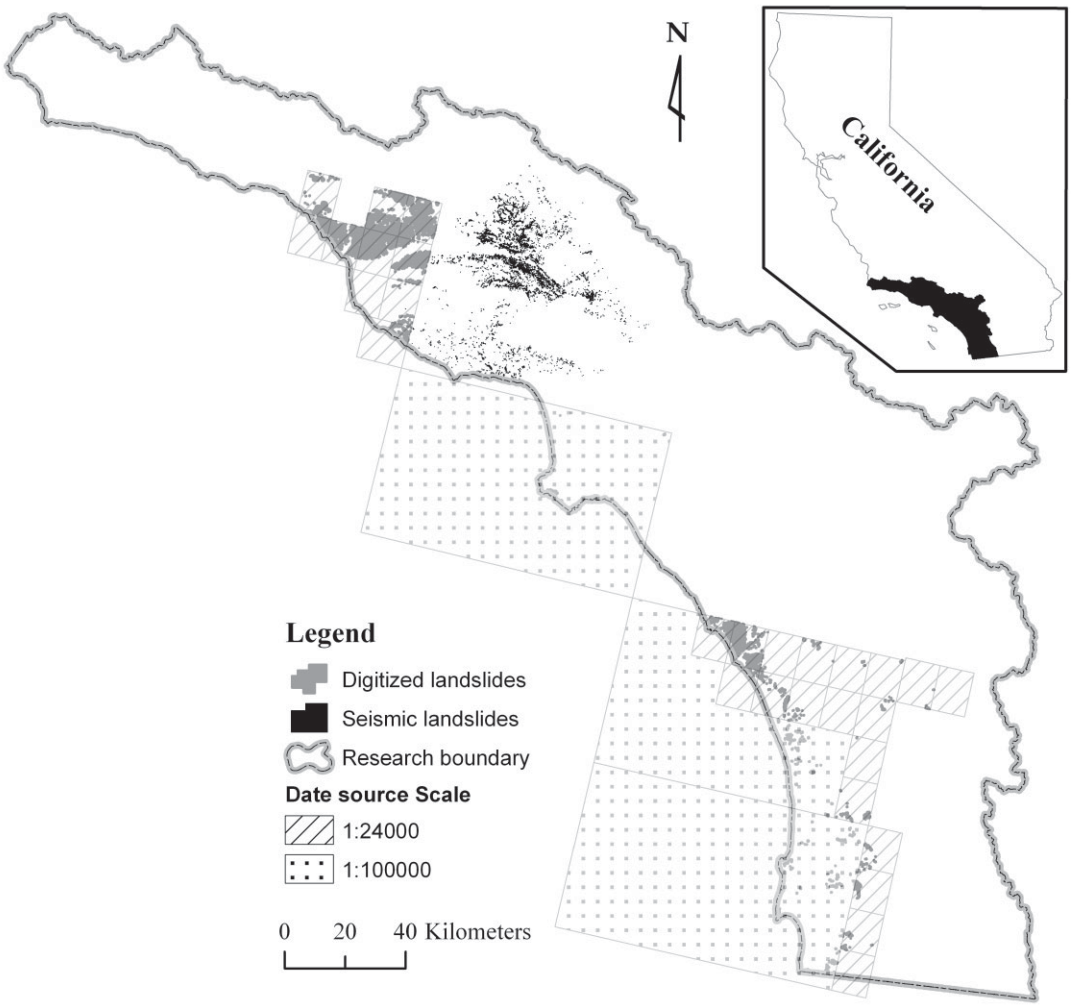


**Figure 2.** Location map and landslide inventories in coastal southern California.

influencing the occurrence of landslides (Dai *et al.*, 2002). Partitioning these factors into categories such as elevations between 500 and 1500 meters above sea level or slopes between 8 and 15 degrees and relating the categories to the probability of landslide occurrence provides a useful basis for assessing regional landslide susceptibility. In the study region, the susceptibility of a given risk factor category was defined as

$$s_{i,j} = \ln\left(\frac{N_{i,j}}{A_{i,j}} \div \frac{N_{\mathrm{T}}}{A_{\mathrm{T}}}\right) \tag{1}$$

where $S_{i,j}$ is the susceptibility of the $j$th category of the $i$th factor, $N_{i,j}$ is the area of landslide scars in the spatial extent associated by $j$th category of the $i$th factor, $A_{i,j}$ is the land area associated with the $j$th category of the $i$th factor and $N_{\mathrm{T}}$ and $A_{\mathrm{T}}$ are the total area of landslide scars and total land area of the study region, respectively. The index of susceptibility ($S$) was used to indicate the weight of an individual category for any risk factor through the comparison of landslide density ($N_{i,j}/A_{i,j}$) in the spatial extent associated by the category with the mean landslide density in the research region. Using Equation (1), spatially distributed datasets (i.e. potential risk factors separated into unique categories) were transformed into susceptibility maps. Given that these maps were raster format (i.e. grid), each pixel was assigned a susceptibility value $S_i$ based on its underlying factor category.

From Equation (1) and the resulting susceptibility map, localized susceptibility varies with factor category (see Table II below). Some categories were highly correlated to landslides, and the areas associated with these categories had high positive susceptibility. Some categories were not correlated to landslides, as indicated by negative susceptibility



DOI: 10.1002/esp

values. For example, areas with steep slopes have much higher susceptibility values than areas with mild or flat slopes. For a risk factor to be useful for susceptibility mapping, its categories should provide a range of susceptibility values. The standard deviation ($\sigma_i$) of the susceptibility for a given categorized risk factor was used as an index to quantify its influence on landsliding:

$$\sigma_i = \sqrt{\frac{\sum_{j=1}^{n}\left(X_{i,j} - \bar{X}_i\right)^2}{n}} \tag{2}$$

where $\sigma_i$ is the standard deviation of the susceptibility of the $i$th factor, $n$ is the number of grid cells in the susceptibility map associated with the $i$th factor, $\bar{X}_i$ is the mean susceptibility of the factor and $x_{i,j}$ is the susceptibility of the $j$th grid cell for the $i$th factor (see Table III below).

Based the dimensionless characteristics of susceptibility, $S_i$, for any given grid cell, it was possible to determine the cumulative susceptibility, $S$, for multiple ($n$) risk factors (or variables) at a given location:

$$S = \frac{1}{n}\sum_{i=1}^{n} S_i \tag{3}$$

The range of $S$ values for a given region was divided into equally sized bins to define susceptibility levels, and each grid cell was assigned a susceptibility level according to its $S$ value (Figures 3 and 4; see Table V below). Using this method, a susceptibility map that integrates multiple risk factors was generated for the region using five categories: very low, low, moderate, high and very high (Figure 4).

A second index, integrated susceptibility ($SI$), was also used to assess the importance of given risk factors:

$$SI = \ln\left(\frac{N_S}{A_S} \div \frac{N_T}{A_T}\right) \tag{4}$$

where $N_S$ is the area of landslide scars in the region associated with a susceptibility level greater than moderate (i.e. high and very high/severe) and $A_S$ is the land area occupied by these susceptibility levels. A factor with a high $SI$ value implies it can be categorized into bins that accurately predict the occurrence and/or non-occurrence of landslides and is more important than factors with lower $SI$ value (see Table III below).

The index of relative landslide density ($R$) as defined by Baeza and Corominas (2001) was used to validate the susceptibility mapping results.

$$R_k = \left[\frac{n_k}{A_k} \div \sum_{i=1}^{m}\frac{n_i}{A_i}\right] \times 100 \tag{5}$$

where $R_k$ is the relative landslide-density of the $k$th susceptibility level, $n_k$ is the area of landslide scars in the $k$th susceptibility level, $A_k$ is the land area occupied by the $k$th susceptibility level, $m$ is the total number of susceptibility levels and $k$ refers to any digit from 1 to $m$. As listed in Tables IV and V below, the landslide density index increases with susceptibility level, suggesting that the distribution of observed landslides is consistent with the assigned susceptibility levels (i.e., areas with higher susceptibility levels have a greater density of landslides).

## Data Analysis

### Landslide inventory

Two landslide inventory datasets were used: (1) geologic maps that include landslide outlines generated during 1999–2006 and (2) seismic landslides triggered by the 1994 Northridge, CA, earthquake (Harp and Jibson, 1995). The GIS-based landslide inventory maps used in this research were created by digitizing landslide boundaries on the 7·5 minute geologic maps at 1:24 000 scale and 30 × 60 minute geologic maps at 1:100 000 scale. The seismic triggered landslide maps at 1:24 000 scale were obtained in a GIS format. Figure 2 and Table I provide a summary of the landslide inventory data.

A total of 5389 landslides were identified and digitized from the geologic maps (Figure 2). Approximately 95% of these landslides were digitized from the 1:24 000 geologic maps. The accuracy of the base map (i.e. the 1:24 000



DOI: 10.1002/esp

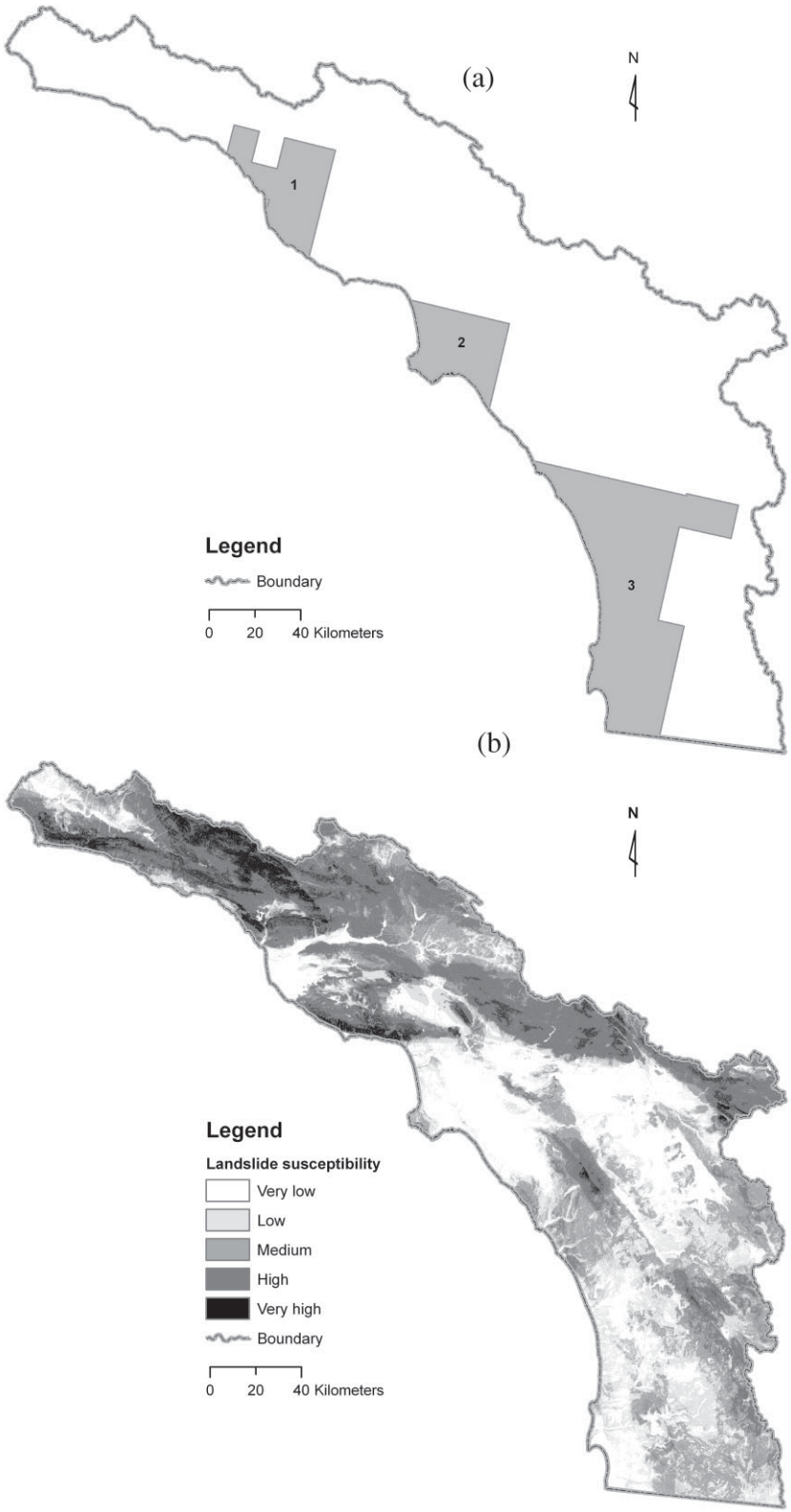


**Figure 3.** (a) Landslide inventory Zones 1–3 and (b) landslide susceptibility map using data only from Zones 1 and 3.



DOI: 10.1002/esp

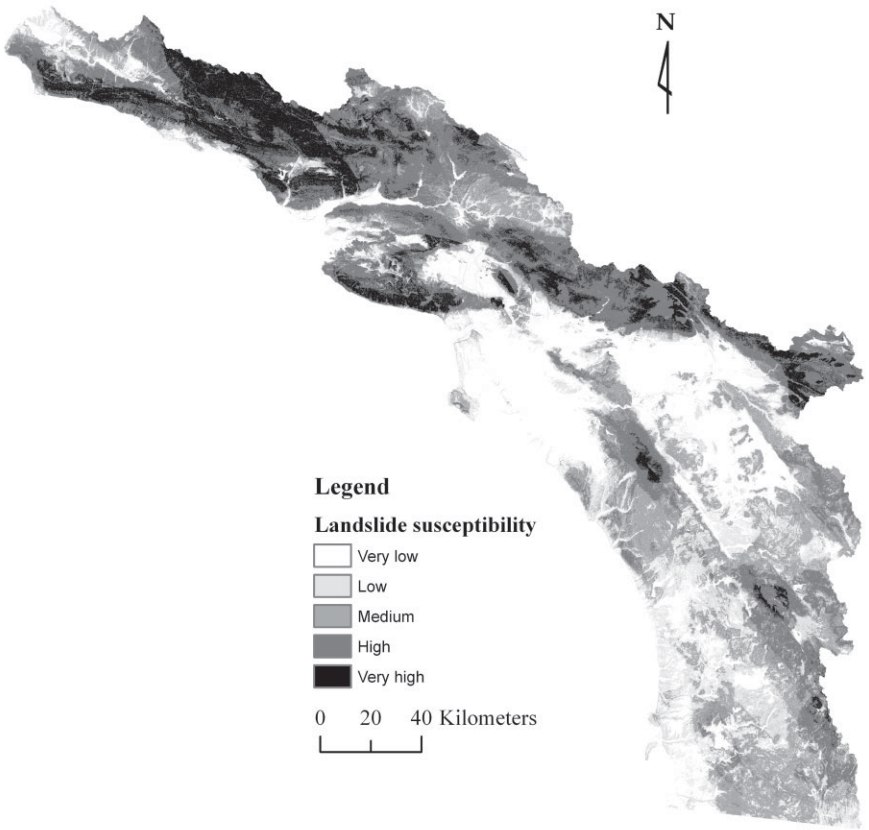


**Figure 4.** Landslide susceptibility map for southern California based on seven factors (in order of importance): ground slope, event precipitation, land cover, surface curvature, proximity to fault lines, ground elevation and proximity to the coastline.

**Table I.** Data sources

| Category | Data source |
|---|---|
| Landslide inventory | (1) 11 111 seismic landslides triggered by 1994 Northridge, California at 1:24 000 scale (Harp and Jibson, 1995); (2) 30 × 60 minute geologic maps of Oceanside (2005), San Diego (2005) and Long Beach (2003) at 1:100 000 scale; (3) 7·5 minute geologic maps of Aguanga (2003), Morro Hill (2001), San Vicente Reservoir (2002), Bonsall (2000), Ojai (2005), Santa Paula (2004), Camarillo (2004), Otay Mesa (2002), Santa Paula Peak (2005), Dana Point (1999), Oxnard (2003), Saticoy (2004), El Cajon (2002), Pala (2000), Temecula (2000), Escondido (1999), Pechanga (2000), Vail Lake (2003), Fallbrook (2000), Pitas Point (2003), Valley Center (1999), Jamul Mountains (2002), Point Mugu (2003), Ventura (2003), Las Pulgas Canyon (2001), San Clemente (1999), White Ledge Peak (2004), Margarita Peak (2001) and San Onofre Bluff (1999) at 1:24 000 scale |
| DEM | US Geological Survey 7·5 minute (30 m) digital elevation models (http://seamless.usgs.gov) |
| Roads | (1) 2002 TIGER line files, railroads and roads, US Census Bureau, Geography Division (http://www.census.gov/geo/www/tiger/index.html); (2) major roads in California, California Spatial Library (http://gis.ca.gov/data.epl) |
| Fault lines | Geology of the conterminous United States at 1:2 500 000 Scale – a digital representation of the 1974 P. B. King and H. M. Beikman map (http://pubs.usgs.gov/dds/dds11/) |
| Land cover | 1990s land cover data for California, California Gap Analysis Project (http://www.biogeog.ucsb.edu/projects/gap/gap_data_state.html) |
| 2-yr, 6-hr precipitation | National Oceanic and Atmospheric Administration (NOAA), National Weather Service, Atlas No. 2 (http://www.nws.noaa.gov/ohd/hdsc/noaaatlas2.htm) and Atlas No. 14 (http://hdsc.nws.noaa.gov/hdsc/pfds/pfds_gis.html) |



DOI: 10.1002/esp

geologic map) was assumed to be within National Map Accuracy Standards, with a horizontal accuracy of 14 m at the 95% confidence level. When the base maps were digitized, the calculated root-mean-square (RMS) error averaged 4·9 m, ranging from 1·2 to 8·7 m. Thus, the accuracy of the 1:24 000 geologic map used to digitize the landslides is approximately ±20 m and no greater than 30 m. Only 5% of the recorded landslides were digitized from the 1:100 000 scale geologic maps. The accuracy of the 1:100 000 base map is approximately 50 m plus the transformed RMS error during the processing of digitization of about 20 m. More than 11 000 seismic landslides (Harp and Jibson, 1995) are shown in the digital inventory map (Figure 2). The location of seismic landslides is accurate within about 15 m, with a maximum error of 30 m. For the 16 500 landslides identified in this research, over 98% were accurate within approximately ±20 m, with 2% accurate within ±70 m (Figure 2).

## Potential landslide risk factors

Numerous landslide risk factors (or parameters, variables) have been used for defining spatial hazard maps (Catani *et al.*, 2005). According to Wu and Sidle (1995), these factors can be grouped into two types: (1) the intrinsic factors that contribute to landslide, such as topography, geology and hydrology, and (2) the extrinsic variables that tend to trigger landslides, such as intense rainfall, earthquakes and landscape modifications (e.g. urbanization, road construction, mining etc.). On the basis of the prevailing characteristics of landslides in southern California (Morton *et al.*, 2003) and the results of a preliminary monovariate statistical analysis of the parameters within mapped landslides, ten potential risk factors were selected: precipitation, elevation, coastline proximity, aspect, slope, curvature, fault proximity, major road proximity, drainage proximity and land cover (Table I). Ground elevation, surface slope, aspect, surface curvature and the drainage network were derived from a 30 m DEM (Table II). The proximity to the coastline, fault lines, major roads and drainage lines were calculated through spatial statistics functions in ESRI's ArcGIS. The rationale for the selected factors is described below. In general, the selected factors focus on rainfall, ground slope and landscape disturbances.

Precipitation is a fundamental slope instability factor. In the study region, Morton *et al.* (2003) found that rainfall can saturate the colluvium to the point of failure above the colluvium–bedrock interface, resulting in a landslide. During winter storms, precipitation is supplied by a flow of atmospheric moisture from the southwest (i.e. offshore to onshore), and steep mountainous terrain near the coastline contributes to significant orographic precipitation (NOAA, 2001). On the windward side of the mountains (south- and west-facing slopes), nearest the coastline, rainfall increases as elevation increases (Beighley *et al.*, 2003). On the leeward side of the mountains (north- and east-facing slopes), rainfall decreases as the distance to the ocean increases. Generally, areas receiving higher rainfall relative to the region have a higher probability of landslide occurrence. Four factors were selected to capture the magnitude and combined spatial and temporal rainfall characteristics: 2-year 6-hour rainfall depth (NOAA Altas Nos 2 and 14), ground elevation, distance to the coastline and aspect.

Ground surface slope is another important driver in landslide analysis (Catani *et al.*, 2005). As slope increases, the probability of landslide occurrence generally increases. This is likely due to the increase of shear stress in the soil or other unconsolidated material as ground slope increases (Lee and Choi, 2004). The effect of surface curvature, which represents the current morphology of the landscape, was also investigated. A positive curvature indicates that the surface is upwardly convex, where a negative curvature indicates that the surface is upwardly concave. A value of zero means the surface is flat. The convex and concave slopes contain more water after a storm and retain this water for a longer period relative to zero curvature slopes, resulting in a higher probability of landslide occurrence (Lee and Talib, 2005).

The proximity of local lineament features (i.e. faults, roads and streams) was used to investigate any cause–effect relationships between lineament and landslide occurrence. The proximity to faults was selected to investigate the effects of varying geologic conditions and potential seismic activity on landsides. The proximity to roads was selected to investigate the effects of altering the natural terrain and drainage system by the mass grading. The proximity to drainage lines or streams was selected to investigate the effects of regional geomorphology and localized processes, such as stream channel erosion (headward and back erosion), on the occurrence of landslides. For all proximity measures, we anticipated the probability of landslide occurrence to be highest near the lineament features.

Land use/land cover also influences slope behavior (Varnes and IAEG, 1984). In southern California, Lee and Choi (2004) found the probability of landslide occurrence to be highest for grass lands and certain forest types, but concluded that their findings may be a result of co-existing landscape characteristics. For example, they show a high probability of landslide occurrence for vegetation types found in steep, mountainous areas. In this effort, land cover was used to investigate potential effects of urbanization (altered drainage networks, landscape alterations, civil infrastructure).



DOI: 10.1002/esp

**Table II.** Categories, area ratios and susceptibilities for potential landslide risk factors

| Potential risk factors | Category | Area ratio (%) | Susceptibility |
|---|---|---|---|
| Elevation (m) | <152 | 19 | −0·83 |
| | 152–457 | 31 | 0·41 |
| | 457–914 | 25 | 0·33 |
| | 914–1219 | 11 | 0·71 |
| | >1219 | 14 | 1·53 |
| Slope (degrees) | <8 | 26 | −3·23 |
| | 8–15 | 12 | −1·08 |
| | 15–25 | 15 | −0·20 |
| | 25–35 | 14 | 0·50 |
| | >35 | 33 | 1·12 |
| Proximity to fault line (km) | <3 | 37 | 0·60 |
| | 3–6 | 24 | 0·35 |
| | 6–10 | 18 | −0·23 |
| | 10–15 | 12 | −0·99 |
| | >15 | 8 | −1·78 |
| 6-hr precipitation (mm) | <33 | 11 | −1·11 |
| (recurrence interval: 2 yrs) | 33–41 | 35 | −0·91 |
| | 41–51 | 24 | 0·33 |
| | 51–64 | 20 | 1·76 |
| | >64 | 10 | 1·47 |
| Proximity to coastline (km) | <5 | 8 | 0·44 |
| | 5–10 | 7 | 0·07 |
| | 10–20 | 14 | −0·34 |
| | 20–30 | 14 | 0·20 |
| | >30 | 57 | −1·12 |
| Profile curvature‡ | <−1·5 | 9 | 0·89 |
| | −1·5 to −0·1 | 30 | 0·15 |
| | −0·1–0·1 | 26 | −1·70 |
| | 0·1–1·5 | 25 | 0·22 |
| | >1·5 | 10 | 0·90 |
| Land cover | developed | 28 | −1·29 |
| | planted/cultivated | 6 | −1·52 |
| | grass | 7 | 0·96 |
| | shrub | 48 | 0·66 |
| | hardwood | 3 | 1·20 |
| | conifer | 7 | −0·33 |
| | water | 0·4 | −3·89 |
| | barren | 0·3 | −2·11 |
| Aspect (degree) | flat | 1 | N/A* |
| | 315–45 | 19 | 0·33 |
| | 45–135 | 18 | 0·12 |
| | 135–225 | 32 | −0·09 |
| | 225–315 | 30 | −0·2 |
| Proximity to major road (km) | <1 | 23 | −1·05 |
| | 1–2 | 17 | −0·17 |
| | 2–3 | 13 | 0·39 |
| | 3–4 | 10 | 0·52 |
| | >4 | 38 | 0·30 |
| Proximity to drainage line (km) | <0·5 | 35 | −0·47 |
| | 0·5–1·0 | 27 | −0·05 |
| | 1·0–1·5 | 19 | 0·20 |
| | 1·5–2·0 | 12 | 0·45 |
| | >2·0 | 7 | 0·65 |

‡ Concave slope, curvature < 0; convex slope, curvature > 0; straight slope, curvature = 0.
* No landslide sites.



DOI: 10.1002/esp

**Table III.** Standard deviation ($\sigma$) and integrated susceptibility (*SI*) for potential landslide risk factors

| Risk factors | $\sigma$ | *SI* |
|---|---|---|
| Slope | 1·73 | 0·92 |
| 2-yr 6-hr storm | 1·12 | 1·02 |
| Land Cover | 1·02 | 0·74 |
| Curvature | 0·95 | 0·35 |
| Proximity to fault | 0·74 | 0·49 |
| Elevation | 0·69 | 0·47 |
| Proximity to coastline | 0·61 | 0·26 |
| Proximity to major road | 0·58 | 0·24 |
| Aspect | 0·39 | 0·09 |
| Proximity to drainage line | 0·37 | 0·20 |

## Risk factor categories

To categorize and quantify the landslide susceptibility of continuous potential risk factors, they were reclassified into five categories (or subclasses) using the following rules: (1) the area ratio of any category must be less than 50%; (2) the area ratio of any category must be greater than 5% and (3) the area ratio of any two categories must be less than 75%. Discrete risk factors (e.g. land cover) were categorized by their natural properties. Using these rules and Equation (1), susceptibility values for all potential risk factor categories were determined (Table II).

## Risk factor selection

Standard deviation (Equation (2)) and integrated susceptibility (Equation (4)) were used to weight the influence of each potential risk factor on the occurrence of landslides. Based on the standard deviation and integrated susceptibility for the ten factors listed in Table III, surface slope and event precipitation (2-year 6-hour precipitation) were the two most important factors for predicting landslide locations in southern California. The next most important factors are land cover, surface curvature, proximity to faults, elevation, proximity to the coastline, proximity to roads, aspect and proximity to drainage lines. In this research, the seven most important factors were selected to map landslide susceptibility: ground slope, event precipitation, land cover, surface curvature, proximity to faults, elevation and proximity to coastline. The remaining three factors were not used due to lack of influence (Tables II and III). The decision for selecting factors for use in the final susceptibility mapping was subjective. For inclusion, a risk factor had to have a standard deviation greater than 50% and integrated susceptibility greater than 25%.

## Susceptibility analysis and validation

Using GIS overlay analysis and Equations (1) and (3), an integrated landslide susceptibility map based on multiple factors was developed. To validate the susceptibility mapping results, the data area was divided into three zones (Figure 3(a)). Using only the data from Zones 1 and 3, susceptibility was determined for Zone 2 (Figure 3(b)). Based on the Zone 2 modeling results, the relative landslide density, *R*, index was substantially larger in areas attributed to high susceptibility levels relative to areas associated with lower susceptibility levels (Table IV). The density of

**Table IV.** Mapping results using the data from Zones 1 and 3 to predict landslides in Zone 2

| Susceptibility level | Cells | Ratio (%) | Cells in Zone 2 | Landslide cells in Zone 2 | $n_i/N_i$ | $R_i$ index |
|---|---|---|---|---|---|---|
| 1 | 827 443 | 26 | 96 901 | 23 | 0·0002 | 0·2 |
| 2 | 603 352 | 19 | 11 785 | 129 | 0·0109 | 7·3 |
| 3 | 762 326 | 24 | 4 522 | 165 | 0·0365 | 24·2 |
| 4 | 820 421 | 26 | 963 | 99 | 0·1028 | 68·3 |
| 5 | 137 871 | 5 | 0 | 0 | N/A | N/A |
| Total | 3 151 413 | 100 | 114 171 | 416 | N/A | N/A |



DOI: 10.1002/esp

**Table V.** Mapping results using the data from all three zones

| Hazard level | Susceptibility | No. of cells | Area ratio | No. of landslide cells† | No. of landslide cells‡ | $R_i$ index |
|---|---|---|---|---|---|---|
| Very low | <–0·60 | 839 677 | 26·6 | 0 | 701 | 0·4 |
| Low | –0·60 to –0·20 | 477 112 | 15·2 | 19 | 3 035 | 3·7 |
| Medium | –0·20–0·20 | 710 243 | 22·5 | 205 | 4 930 | 6·7 |
| High | 0·20–0·60 | 791 138 | 25·1 | 1898 | 12 036 | 34·5 |
| Very high | >0·60 | 333 243 | 10·6 | 237 | 9 361 | 54·6 |

† Earthquake triggered landslide.
‡ Digitized landslide.

observed landslides was positively correlated to high susceptibility levels. Thus, our mapping approach and defined susceptibility levels based on Zones 1 and 3 provide a reasonable comparison to the observed landslide locations in Zone 2. A regional assessment is provided in the Discussion section.

## Results

Using Equations (1) and (3) and the landslide data from all three zones, landslide susceptibilities for all seven risk factors were generated for southern California. The values of susceptibility were divided into five equally sized segments (Table V) to define susceptibility levels: very low, low, moderate, high and very high. Each grid cell was then assigned to a susceptibility level according to its susceptibility value (Figure 4). From the susceptibility map, the land areas with high and very high landslide susceptibility occupy 26% of the total study area, while accounting for approximately 71% of the digitized landslide scars and 90% of the seismic landslide scars. These areas mostly have surface slopes greater than 46% (25°) and 2-year, 6-hour precipitation greater than 51 mm (2·0 in). The land areas associated with low and very low landslide susceptibility occupy 42% of total research area, while accounting for only 12% of digitized landslides and less than 1% of recorded seismic landslides. These areas mostly have slopes less than 27% (15°) and 2-year, 6-hour precipitations less than 41 mm (1·6 in).

## Discussion

The susceptibility map shown in Figure 4 is based on seven spatially distributed datasets. While it is likely that additional data can be associated with the occurrence or non-occurrence of landslides, this research focuses on datasets that are commonly available throughout the United States. For example specific soil properties and areas that have been severely burned by forest fires are likely to be potential risk factors for landslides. For soil data, a key problem in mapping landslide susceptibility is categorizing unique soil properties. This process requires high-resolution data with properties that correlate to known landslide locations. At the national level, the State Soil Geographic (STATSGO) Database does not provide the required resolution. The Soil Survey Geographic (SSURGO) Database, which provides a much higher resolution, was not available for the entire study region. Guimarães *et al.* (2003) suggests that the acquisition of high-quality digital elevation models is more important than the generation of spatially distributed soil properties for basin or regional scale assessment of shallow landslide hazards. Thus, soil data was not used for mapping landslide susceptibility. When available, future efforts will investigate the potential use of the SSURGO database.

Wildfires are common to southern California, and likely result in the destabilization of pre-existing deep-seated landslides over long time periods (Cannon *et al.*, 1998). The expansion of urban development into forested areas has created a situation where wildfires can adversely affect lives and property directly or by the flooding and landslides that occur in the aftermath of fires. Post-fire landslide hazards include fast-moving, highly destructive debris flows that can occur in the years immediately after wildfires in response to high-intensity rainfall events. Additional landslides can result over longer time periods due to root decay and loss of soil strength (Cannon *et al.*, 2004). Thus, the locations of past wildfires are likely a potential risk factor for predicting landslides. However, to properly utilize the influence of wildfire on landslide susceptibility mapping requires both the date of wildfire occurrence and any resulting landslides. In this research, most recorded landslides occurred before 2000, while most spatially distributed wildfire data



DOI: 10.1002/esp

are for periods after 2000. Thus, wildfires were not used to generate the presented landslide susceptibility map. Future efforts will investigate the applicability of soil and wildfire data in regional scale landslide susceptibility mapping.

Assessing the presented susceptibility mapping approach is challenging. The relative landslide density, *R*, index and known landslide locations from three different zones were previously used to show the generally positive performance of the mapping methods. As a second assessment, the mapping results (Figure 4) were also compared with a recent USGS susceptibility mapping project (Morton *et al.*, 2003). Morton *et al.* (2003) utilized three risk parameters, geology, slope and aspect, to map four landslide susceptibility levels: none, low, moderate and high. For the comparison, the five susceptibility levels shown in Figure 4 were matched to the four USGS levels using on following: very low to none; low to low; medium to moderate; high plus very high to high. Based on the extent of the USGS mapping region, our predicted susceptibility levels agreed with the USGS levels for 44% of the area, while cells differing by only one level accounting for an additional 30% of the area. Thus, 74% of the comparison region was within one susceptibility level. Overall, our approach tended to produce more areas with high and very high susceptibilities, which is likely due to the inclusion of additional risk factors such as event precipitation and differences in landslide inventories.

## Conclusions

In this paper, landslide susceptibility modeling indexes were developed to quantify and weight the influence of potential risk factors for predicting the locations of landslides. Using GIS, a multivariate statistical approach for landslide susceptibility mapping was developed. Modeling results for southern California suggest that ground slope and event precipitation are the most important landslide risk factors, followed by land cover, surface curvature, proximity to faults, elevation and proximity to the coastline.

As part of this research, a new GIS-based landslide inventory was produced for southern California containing 5389 landslide scars digitized from the existing geologic maps. An additional 11 111 seismic landslide scars collected from previous research were also used. The developed landslide susceptibility maps show that areas classified as having high or very high susceptibilities contain 71% of the digitized landslide scars and 90% of the seismic landslide scars while only occupying 26% of the total study area. These areas can be generalized as having steep slopes (>46%) and intense rainfall (2-year, 6-hour precipitation >51 mm). Only 12% of digitized landslides and less than 1% of recorded seismic landslides were located in the areas classified as having low or very low susceptibility, while occupying 42% of the total study region. These areas generally have ground slopes less than 27% and 2-year, 6-hour precipitation less than 41 mm (1·6 in). Relative to previous susceptibility mapping results, the presented approach provides comparable results, with an increase in regions having high and very high susceptibilities. These differences may be attributed to the use of additional risk parameters, specifically event precipitation, and different landslide inventories.

## References

Aleotti P, Baldelli P, Polloni G, Puma F. 1998. Keynote paper: Different approaches to landslide hazard assessment. *Proceedings of the Second Conference on Environmental Management (ICEM-2)*, Wollongong, Australia, 1998, Vol. 1; 3–10.

Aleotti P, Chowdhury R. 1999. Landslide hazard assessment: summary review and new perspectives. *Bulletin of Engineering Geology and the Environment* **58**: 21–44.

Anbalagan R, Singh B. 1996. Landslide hazard and risk assessment mapping of mountainous terrains – a case study from Kumaun Hymalaya, India. *Eng Geol* **43**: 237–246.

Atkinson PM, Massari R. 1998. Generalized linear modeling of landslide susceptibility in the central Apennines, Italy. *Computers and Geosciences* **24**: 373–385.

Baeza C, Corominas J. 2001. Assessment of shallow landslide susceptibility by means of multivariate statistical techniques. *Earth Surface Processes and Landforms* **26**: 1251–1263.

Beighley RE, Melack JM, Dunne T. 2003. Impacts of climatic regimes and urbanization on streamflow in California coastal watersheds. *Journal of the American Water Resources Association* **29**: 1419–1433.

Bernknopf RL, Campbell RH, Brookshire DS, Shapiro CD. 1988. A probabilistic approach to landslide hazard mapping in Cincinnati, Ohio, with applications for economic evaluation. *Bulletin of the American Association of Engineering Geologists* **25**: 39–56.

Brabb EE. 1984. Innovative approach to landslide hazard and risk mapping. *Proceedings of the 4th International Symposium on Landslides*, Toronto, Vol. 1; 307–324.

Cannon SH, Ellis WL, Godt JW. 1998. *Evaluation of the Landslide Potential in Capulin Canyon Following the Dome Fire, Bandelier National Monument, New Mexico*, US Geological Survey Open-File Report 98-42.

Cannon SH, Gartner JE, Rupert MG, Michael JA. 2004. *Emergency Assessment of Debris-Flow Hazards from Basins Burned by the Cedar and Paradise Fires of 2003, Southern California*, US Geological Survey Open-File Report 2004-1011.



DOI: 10.1002/esp

Carrara A. 1983. Multivariate methods for landslide hazard evaluation. *Mathematical Geol* **15**: 403–426.
Catani F, Casagli N, Ermini L, Righini G, Menduni G. 2005. Landslide hazard and risk mapping at catchment scale in the Arno River Basin. *Landslide* **2**: 329–342.
Chang KT, Liu JK. 2004. Landslide features interpreted by neural network method using a high-resolution satellite image and digital topographic data. In Proceedings of XXth ISPRS Congress, *Geo-Imagery Bridging Continents*, Istanbul, 2004; 574–579.
Collins BD, Znidarcic D. 2004. Stability analyses of rainfall induced landslides. *Journal of Geotechnical and Geo-Environmental Engineering* **130**(4): 362–372.
Dai FC, Lee CF, Ngai YY. 2002. Landslide risk assessment and management: an overview. *Eng Geol* **64**: 65–87.
Fall M, Azzam R, Noubactep C. 2006. A multi-method approach to study the stability of natural slopes and landslide susceptibility mapping. *Engineering Geology* **82**: 241–263.
Fenti V, Silvano S, Spagna V. 1979. Methodological proposal for an engineering geomorphological map, forecasting rockfalls in the Alps. *Bull of the Int Assoc Eng Geol* **19**: 134–138.
Guimarães RF, Montgomery DR, Greenberg HM, Fernandes NF, Gomes RAT, Júnior OADC. 2003. Parameterization of soil properties for a model of topographic controls on shallow landsliding: application to Rio De Janeiro. *Engineering Geology* **69**: 99–108.
Gupta RP, Joshi BC. 1989. Landslide hazard zoning using the GIS approach – a case study from the Ramganga catchment, Himalayas. *Engineering Geology* **28**: 119–131.
Gupta P, Anbalagan R. 1997. Slope stability of Theri Dam Reservoir Area, India, using landslide hazard zonation (LHZ) mapping. *Quarterly Journal of Eng Geology* **30**: 27–36.
Guzzetti F, Carrarra A, Cardinali M, Reichenbach P. 1999. Landslide hazard evaluation: a review of current techniques and their application in a multi-scale study, Central Italy. *Geomorphology* **31**: 181–216.
Guzzetti F, Reichenbach P, Cardinali M, Galli M, Ardizzone F. 2005. Probabilistic landslide hazard assessment at the basin scale. *Geomorphology* **72**: 272–299.
Hammond C, Hall D, Miller S, Swetik P. 1992. *Level I Stability Analysis (LISA) Documentation for Version 2*, General Technical Report INT-285, USDA Forest Service Intermountain Research Station; 121.
Harp EL, Jibson RW. 1995. *Inventory of Landslides Triggered by the 1994 Northridge, California Earthquake*, USGS Open-File Report 95-213.
Iverson RM. 2000. Landslide triggering by rain infiltration. *Water Resources Research* **36**(7): 1897–1910.
Jibson RW. 2001. *Probabilistic Landslide Hazard Assessment*, Geological Survey Open-File Report 01-324; 41–46.
Jibson RW, Harp EL, Michael JA. 1998. *A Method for Producing Digital Probabilistic Seismic Landslide Hazard Maps: an Example from Southern California*, US Geological Survey Open-File Report 98-113; 17, 2pl.
Kienholz H. 1978. Maps of geomorphology and natural hazard of Griendelwald, Switzerland, scale 1:10 000. *Artic and Alpine Research* **10**: 169–184.
Lee S, Choi J. 2004. Landslide susceptibility mapping using GIS and the weight-of-evidence model. *Int. J. Geographical Information Science* **18**: 789–814.
Lee S, Ryu JH, Min K, WJS. 2003. Landslide susceptibility analysis using GIS and artificial neural network. *Earth Surface Processes and Landforms* **28**: 1361–1376.
Lee S, Talib JA. 2005. Probabilistic landslide susceptibility and factor effect analysis. *Environmental Geology* **47**: 982–990.
Leroi E. 1997. Landslide risk mapping: problems, limitation and developments. In *Landslide Risk Assessment*, Cruden D, Fell R (eds). Balkema: Rotterdam; 239–250.
Montgomery DR, Dietrich WE. 1994. A physically based model for topographic control on shallow landsliding. *Water Resources Research* **30**(4): 1153–1171.
Morton DM, Alvares RM, Campbell RH. 2003. *Preliminary Soil-Slip Susceptibility Maps, Southwestern California*, US Geological Survey Open-File Report 03-17.
Naranjo JL, VanWesten CJ, Soeters R. 1994. Evaluating the use of training areas in bivariate statistical landslide hazard analysis: a case study in Colombia, ITC Journal 1994-3, 292–300.
Nash D. 1987. A comparative review of limit equilibrium methods of slope stability analysis. In *Slope Stability*, Anderson MG, Richards KJ (eds). Wiley: New York; 11–75.
National Oceanic and Atmospheric Administration (NOAA). 2001. *Sulphur Mountain Doppler Radar: a Performance Study*, Technical Memorandum NWS WR-267. National Weather Service, Los Angeles Weather Service: Oxnard, CA.
National Research Council (NRC). 2004. *Partnerships for Reducing Landslide Risk: Assessment of the National Landslide Hazards Mitigation Strategy*. National Academies Press: Washington, DC; 131.
Pack RT, Tarboton DG, Goodwin CN. 1999. GIS-based landslide susceptibility mapping with SINMAP. In *Proceedings of the 34th Symposium on Engineering Geology and Geotechnical Engineering*, Bay JA (ed.). Vol. 34; 219–231.
Rupke J, Cammeraat E, Seijmonsbergen AC, van Westen CJ. 1988. Engineering geomorphology of Widentobel Catchment, Appenzell and Sankt Gallen, Switzerland: a geomorphological inventory system applied to geotechnical appraisal of slope stability. *Engineering Geology* **26**: 33–68.
Selby WA. 2000. *Rediscovering the Golden State: California Geography*. Wiley: New York; 78.
Soeters R, Van Westen CJ. 1996. Slope stability: recognition, analysis and zonation. In *Landslides: Investigation and Mitigation*, Transportation Research Board, National Research Council Special Report 247, Turner AK, Shuster RL (eds); 129–177.
Stevenson PC. 1977. An empirical method for the evaluation of relative landslide risk. *Bull Int Ass Eng Geol* **16**: 69–72.
Terlien MTJ, Van Asch ThWJ, Van Westen CJ. 1995. Deterministic modeling in GIS-based landslide hazard assessment. In *Geographical Information Systems in Assessing Natural Hazards*, Carrar A, Guzzetti F (eds). Kluwer: London; 57–77.



DOI: 10.1002/esp

Van Westen CJ. 2004. Geo-information tools for landslide risk assessment: an overview of recent developments. In *Landslides: Evaluation and Stabilization*, Vol. 1, Lacerda WA, Ehrlich M, Fontoura SAB, Sayao ASF (eds). Balkema: London; 39–56.

Van Westen CJ, Rengers N, Terlien MTJ. 1997. Prediction of the occurrence of slope instability phenomena through GIS-based hazard zonation. *Geologische Rundschau* **86**: 4004–4414.

Varnes DJ, IAEG Commission on Landslides. 1984. *Landslide Hazard Zonation, a Review of Principles and Practice*. UNESCO: Paris.

Wachal DJ, Hudak PF. 2000. Mapping landslide susceptibility in Travis County, Texas, USA. *GeoJournal* **51**: 245–253.

Ward TJ, Li RM, Simons DB. 1981. *Use of a Mathematical Model for Estimating Potential Landslide Sites in Steep Forested Drainage Basins*, IAHS Publication 132; 21–41.

Wilson RC, Keefer DK. 1983. Dynamic analysis of a slope failure from the 6 August 1979 Coyote Lake. *California, earthquake: Bulletin of the Seismological Society of America* **73**: 863–877.

Wu W, Sidle RC. 1995. A distributed slope stability model for steep forested basins. *Water Resources Research* **31**: 2097–2110.